








[View Journal Online](#)  
[View Article Online](#)

# Synthesis, crystal structure, and theoretical studies of a macrocyclic silver(I) complex of imino-pyridyl Schiff base ligand

Jahangir Mondal <sup>1</sup>, Meman Sahu <sup>1</sup>, Bhaskar Sharma <sup>1</sup>, Rakesh Ganguly <sup>2</sup>, Shubhamoy Chowdhury <sup>3</sup> and Goutam Kumar Patra <sup>1,\*</sup>

<sup>1</sup> Department of Chemistry, Faculty of Physical Sciences, Guru Ghasidas Vishwavidyalaya, Bilaspur, Chhattisgarh, 495009, India  
[mailtobapi88@gmail.com](mailto:mailtobapi88@gmail.com) (J.M.), [memansahu8@gmail.com](mailto:memansahu8@gmail.com) (M.S.), [bsharma05@gmail.com](mailto:bsharma05@gmail.com) (B.S.), [goutam.patra@ggu.ac.in](mailto:goutam.patra@ggu.ac.in) (G.K.P.)

<sup>2</sup> Shiv Nadar University, Greater Noida, Gautam Buddha Nagar, Uttar Pradesh, 201314, India  
[rakesh.ganguly@snu.edu.in](mailto:rakesh.ganguly@snu.edu.in) (R.G.)

<sup>3</sup> Department of Chemistry, University of Gour Banga, Malda, West Bengal, 732103, India  
[shubha103@yahoo.com](mailto:shubha103@yahoo.com) (S.C.)

\* Corresponding author at: Department of Chemistry, Faculty of Physical Sciences, Guru Ghasidas Vishwavidyalaya, Bilaspur, Chhattisgarh, 495009, India.  
 e-mail: [goutam.patra@ggu.ac.in](mailto:goutam.patra@ggu.ac.in) (G.K. Patra).

## RESEARCH ARTICLE



doi: 10.5155/eurjchem.12.3.248-255.2091

Received: 29 January 2021

Received in revised form: 14 March 2021

Accepted: 30 April 2021

Published online: 30 September 2021

Printed: 30 September 2021

## KEYWORDS

DFT  
 Ag(I) dimer  
 Photophysics  
 Imino-pyridyl ligand  
 X-ray crystal structure  
 Hirshfeld surface studies

## ABSTRACT

The synthesis and characterization of an imino-pyridyl ligand *N,N'*-(butane-1,4-diyl)bis(1-pyridin-2-yl)methanimine (L) and its Ag(I)ClO<sub>4</sub> complex (I) by various spectroscopic techniques and elemental analyses is presented in this study. X-ray single crystal structure of complex I revealed that in complex I, each Ag(I) ion is tetra coordinated with two pyridine N-atoms and two imine N-atoms of the ligand L, forming a macrocyclic dimeric Ag(I) grid. In the macrocyclic dimer complex I, Ag-Ag separation along the chain is 5.318 Å. The Ag-N<sub>py</sub> average distance is 2.396 Å and that of the Ag-N<sub>im</sub> is 2.257 Å. The macrocyclic dimer complex I is supramolecularly arranged by  $\pi$ -stacking interactions. Computational, Hirshfeld surface analysis and photophysical studies on ligand L and complex I have also been performed. Crystal data for C<sub>32</sub>H<sub>36</sub>Ag<sub>2</sub>Cl<sub>2</sub>N<sub>8</sub>O<sub>8</sub> (*M* = 947.33 g/mol): Triclinic, space group P-1 (no. 2), *a* = 9.1714(12) Å, *b* = 10.4373(14) Å, *c* = 10.8297(14) Å,  $\alpha$  = 112.317(3)°,  $\beta$  = 91.391(3)°,  $\gamma$  = 92.353(3)°, *V* = 957.3(2) Å<sup>3</sup>, *Z* = 1, *T* = 293.15 K,  $\mu$ (MoK $\alpha$ ) = 1.220 mm<sup>-1</sup>, *D*<sub>calc</sub> = 1.643 g/cm<sup>3</sup>, 10248 reflections measured (4.07° ≤ 2 $\theta$  ≤ 53.098°), 3966 unique (*R*<sub>int</sub> = 0.0280, *R*<sub>sigma</sub> = 0.0331) which were used in all calculations. The final *R*<sub>1</sub> was 0.0722 (*I* > 2 $\sigma$ (*I*)) and *wR*<sub>2</sub> was 0.2229 (all data).

Cite this: *Eur. J. Chem.* 2021, 12(3), 248-255

Journal website: [www.eurjchem.com](http://www.eurjchem.com)

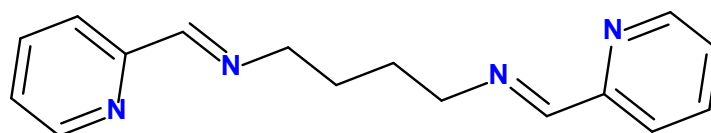
## 1. Introduction

Schiff base complexes have remained an imperative and popular area of research due to their simple synthesis, versatility and diverse range of applications [1]. Among coordination compounds, *d*<sup>10</sup> metal complexes are of interest due to their high thermal stability and good photoluminescent and electro-luminescent properties [2-7].

Silver is an important precious metal and it has been widely used in industry, for example electrical and electronic applications, photographic production and the manufacturing of fungicides [8-17]. The complexation of Ag(I) in a range of supramolecular materials has received increasing attention, due to the coordinative flexibility of the *d*<sup>10</sup> ion as well as to its well-documented tendency to form strong complexes with nitrogen donor ligands [18]. Many topologically promising architectures have been constructed for the Ag(I) ion with bidentate building blocks containing a nitrogen donor [19,20]. Silver(I) possesses high affinity towards N, P, and O donor ligands. However, it prefers N donors over O donor sites in

presence of other hard metal ions and therefore, various heterometallic or bimetallic coordination polymers containing Ag(I) have been successfully synthesized [21-24]. Like 2,2'-bipyridine and 1,10-phenanthroline, Schiff bases derived from 2-pyridine-carboxaldehyde provide the *p*-acidic  $\alpha,\alpha'$ -diimine fragment for metal coordination [25].

Among the coordination compounds of various metals, silver(I) complexes are a theme of interest as luminescent compounds with a wide range of photophysical and photo-chemical properties. Sensitivity of silver(I) complexes to such external stimuli as solvent vapors, mechanical grinding, and temperature make them appealing candidates for the design of smart luminescent materials. Various relaxation mechanisms of the excited states have been established for silver(I) complexes, e.g., fluorescence, phosphorescence, and thermally activated delayed fluorescence (TADF). The excited state lifetimes of silver(I) complexes range from nanoseconds up to micro- and milli-seconds.



Scheme 1. Ligand system (L) used in the study.

In comparison with other types of emission sensitivity to external stimuli, the excitation wavelength-dependent photoluminescence is a rare property for silver(I) complexes.

Analysis of the self-assembly through various intermolecular interactions like hydrogen bonding or  $\pi$ - $\pi$  stacking is important to understand how molecules interact with their direct environment and focus on insights into crystal packing behavior. Hirshfeld surface-based tools appear as a novel approach to this end. The central element in this method is the derivation of the Hirshfeld surface and the immediately interpretable visualization of a molecule within its environment, and the decomposition of this surface to provide a directly accessible 2D map as "molecular fingerprint".

As a part of our ongoing research to study a series of supramolecular complexes of imino-pyridyl Schiff-base ligand and  $d^{10}$ -metal ions as building blocks [26-28], we have presented here the synthesis, structure, photophysical properties and computational study of a novel  $N,N$ -donor Schiff base imino-pyridyl ligand **L** (Scheme 1) and its macrocyclic Ag(I) complex (**I**).

## 2. Experimental

### 2.1. Materials and physical measurements

All chemicals used in this study were purchased from Aldrich Chemical Company, USA, and Acros Chemical Company, USA, and used without further purification unless otherwise mentioned. The melting point was determined by an electrothermal IA9000 series digital melting point apparatus and is uncorrected. Microanalyses were carried out using a Perkin-Elmer 2400II elemental analyzer. Infrared (IR) spectra and solution electronic spectra were recorded on Nicolet Magna IR (Series II) and Shimadzu UV-160A spectrophotometers, respectively.  $^1\text{H}$  NMR spectra and electro-spray ionization mass (ESI-MS) measurements were made using a Bruker Advance 400 MHz NMR Spectrometer and Finnigan LCQ Decapx MAX mass spectrometer, respectively. Fluorescence spectra were recorded on a Perkin Elmer LS55 Luminescence Spectrometer.

### 2.2. Synthesis of the ligand

Ligand was prepared by following a reported procedure [26]. 1,4-Diaminobutane (0.088 g, 1 mmol) was dissolved in anhydrous methanol (15 mL) and to this solution 2 mmol (0.215 g) 2-pyridinecarboxaldehyde was added. The reaction mixture was heated under reflux maintaining a dry condition for 3 h. Then it was kept in air for 24 h. The obtained off-white solid was re-crystallized from methanol.

$N,N'$ -(Butane-1,4-diylium)bis(1-(pyridin-2-yl)methanimine) (**L**): Color: Off-white. Yield: 72%. M.p.: 62-64 °C. FT-IR (KBr,  $\nu$ ,  $\text{cm}^{-1}$ ): 3431 (b), 3055(b), 2937(m), 2854(m), 1649(s), 1587(s), 1469(m), 1437 (s), 1342(m), 1305(s), 1257(m), 1143(vs), 1122(vs), 1087(vs), 1001(m), 867(m), 775(vs), 744(s), 628(vs), 493(s), 406(s).  $^1\text{H}$  NMR (400 MHz,  $\text{CDCl}_3$ ,  $\delta$ , ppm): 8.57 (d, 2H, Ar-H), 8.31 (s, 2H, -CH=N), 7.92 (d, 2H, Ar-H), 7.67 (t, 2H, Ar-H), 7.22-7.27 (m, 2H, Ar-H), 3.60 (t, 4H, -CH<sub>2</sub>), 1.66 (q, 4H, -CH<sub>2</sub>). MS (EI,  $m/z$  (%)): 267.31 ( $\text{LH}^+$ , 100%). Anal. calcd. for  $\text{C}_{16}\text{H}_{18}\text{N}_4$ : C, 72.15; H, 6.81; N, 21.04. Found: C, 71.96; H, 6.69; N, 22.04%.

### 2.3. Synthesis of the complex $[\text{Ag}_2\text{L}_2](\text{ClO}_4)_2(\text{I})$

To 20 mL off-white methanol solution of **L** (0.27 g, 1 mmol) was added solid  $\text{AgClO}_4$  (0.21 g, 1 mmol). The reaction mixture was stirred for 3 h. Light yellow colored precipitate obtained was filtered off and dried in air. It was then dissolved in acetonitrile and kept in the refrigerator overnight. Light yellow crystalline complexes suitable for X-ray analysis were obtained, filtered off, washed with 5 mL methanol dried in vacuum over fused  $\text{CaCl}_2$ . Color: Light yellow. Yield: 60%. FT-IR (KBr,  $\nu$ ,  $\text{cm}^{-1}$ ): 3429 (wb), 3037 (w), 2943 (m), 2856 (m), 2015 (w) 1645 (s), 1615 (s), 1458 (w), 1412 (m), 1318 (w), 1245 (m), 1107 (s), 825 (s), 629 (s), 498 (w). Anal. calcd. for  $\text{C}_{32}\text{H}_{36}\text{N}_8\text{Ag}_2\text{Cl}_2\text{O}_8$ : C, 40.57; H, 3.83; N, 11.83. Found: C, 40.65; H, 3.92; N, 11.76%.

**CAUTION!** Although while working with the perchlorate complex described here, we have not met with any incident, care should be taken in handling them as perchlorates are potentially explosive. They should not be prepared and stored in large amounts.

### 2.4. X-ray crystallography

X-ray single-crystal data are collected using  $\text{MoK}\alpha$  ( $\lambda = 0.7107 \text{ \AA}$ ) radiation on a Bruker APEX II diffractometer equipped with CCD area detector. Data collection, data reduction, structure solution/refinement are carried out using the software package of SMART APEX [29]. The structures are solved by direct methods (SHELXS-97) and standard Fourier techniques and refined on  $F^2$  using full-matrix least-squares procedures (SHELXL-97) using the SHELX-97 package [30] incorporated in WinGX [31]. Generally, non-hydrogen atoms are considered anisotropically. In the crystal structure of complex **I**, hydrogen atoms were introduced in the riding mode. In other cases, the hydrogen atoms are geometrically fixed. The crystallographic details of complex **I** have been summarized in Table 1, and the selected bond lengths and angles of complex **I** have been listed in Table 2.

### 2.5. Theoretical calculations

The program package GAUSSIAN-09 Revision C.01 was used for all calculations [32]. The gas phase geometries of the compound were fully optimized symmetry restrictions in the singlet ground state with the gradient-corrected DFT level coupled with B3LYP [33]. The LanL2DZ basis set was used for the **L** and **I** [34]. The HOMOs and LUMOs of the **L** and **I** were calculated with the TD-DFT method, and the solvent effect (in acetonitrile) was simulated using the polarizing continuum model with the integral equation formalism (C-PCM) [35,36].

### 2.6. Hirshfeld surface calculation

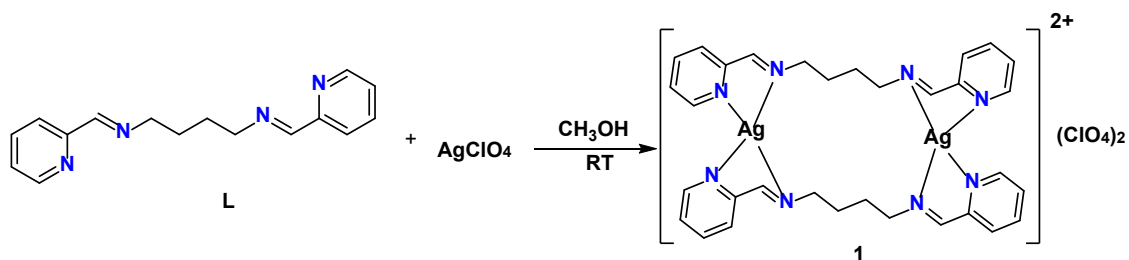
For obtaining additional insight into the intermolecular interaction of molecular crystals, Hirshfeld surface analysis helps as a powerful set-up. The size and shape of Hirshfeld surface allow the qualitative and quantitative study and imaging of intermolecular close contacts in molecular crystals [37]. The Hirshfeld surface enclosing a molecule is defined by a set of points in 3D space where the contribution to the electron density from the molecule of interest is equal to the contribution from all other molecules.

**Table 1.** Crystal data and structure refinement for complex I.

Empirical formula	C <sub>32</sub> H <sub>36</sub> Ag <sub>2</sub> Cl <sub>2</sub> N <sub>8</sub> O <sub>8</sub>
Formula weight	947.33
Temperature (K)	293.15
Crystal system	Triclinic
Space group	P-1
a (Å)	9.1714(12)
b (Å)	10.4373(14)
c (Å)	10.8297(14)
α (°)	112.317(3)
β (°)	91.391(3)
γ (°)	92.353(3)
Volume (Å <sup>3</sup> )	957.3(2)
Z	1
ρ <sub>calc</sub> (g/cm <sup>3</sup> )	1.643
μ (mm <sup>-1</sup> )	1.220
F(000)	476.0
Crystal size (mm <sup>3</sup> )	0.16 × 0.14 × 0.1
Radiation	MoKα (λ = 0.71073)
2θ range for data collection (°)	4.07 to 53.098
Index ranges	-11 ≤ h ≤ 11, -13 ≤ k ≤ 13, -13 ≤ l ≤ 13
Reflections collected	10248
Independent reflections	3966 [R <sub>int</sub> = 0.0280, R <sub>sigma</sub> = 0.0331]
Data/restraints/parameters	3966/1124/422
Goodness-of-fit on F <sup>2</sup>	1.046
Final R indexes [I ≥ 2σ (I)]	R <sub>1</sub> = 0.0722, wR <sub>2</sub> = 0.2098
Final R indexes [all data]	R <sub>1</sub> = 0.0853, wR <sub>2</sub> = 0.2229
Largest diff. peak/hole (e Å <sup>-3</sup> )	1.16/-0.77
CCDC number	2058296

**Table 2.** Experimental (X-ray) and theoretical bond distances (Å) and angles (°) for complex I.

Atom	Atom	Length (Å)	Calc. (Å)	Atom	Atom	Atom	Angle (°)	Calc. (°)	Atom	Atom	Atom	Angle (°)	Calc. (°)
Ag1	N1	2.426(12)	2.4533	N13	Ag1	N1	107.1(6)	141.301	C14	C13	C12	120.0	119.079
Ag1	N13	2.302(13)	2.3327	N13	Ag1	N14	71.9(4)	72.007	C15	C14	C13	120.0	118.825
Ag1	N2	2.234(13)	2.3337	N2	Ag1	N1	72.6(4)	72.017	C14	C15	C16	120.0	118.791
Ag1	N14	2.335(12)	2.4550	N2	Ag1	N13	158.9(7)	136.136	C15	C16	N4	120.0	122.481
N1	C1	1.3900	1.3518	N2	Ag1	N14	120.3(6)	141.168	N3	C11	C12	124.9(13)	122.567
N1	C5	1.3900	1.3658	N14	Ag1	N1	146.8(6)	101.846	C10	N3	Ag1A	127.0(10)	124.672
C1	C2	1.3900	1.4112	C1	N1	Ag1	129.4(5)	129.203	C11	N3	C10	115.4(13)	119.793
C2	C3	1.3900	1.4112	C1	N1	C5	120.0	118.934	C11	N3	Ag1A	116.5(10)	115.533
C3	C4	1.3900	1.4079	C5	N1	Ag1	109.3(5)	111.510	N12	C110	C109	93.7(11)	110.301
C4	C5	1.3900	1.4089	N1	C1	C2	120.0	122.481	N13	C107	C108	86.2(10)	110.301
C5	C6	1.396(15)	1.4788	C3	C2	C1	120.0	118.791	C109	C108	C107	118.0(12)	112.106
C6	N2	1.260(16)	1.2949	C4	C3	C2	120.0	118.825	C110	C109	C108	125.4(12)	112.107
C7	C8	1.450(16)	1.5499	C3	C4	C5	120.0	119.079	C6	N2	Ag1	115.4(9)	115.536
C7	N2	1.386(16)	1.4826	N1	C5	C6	116.1(8)	117.819	C6	N2	C7	120.2(13)	119.795
C8	C9	1.522(14)	1.5445	C4	C5	N1	120.0	121.890	C7	N2	Ag1	121.1(11)	124.669
C9	C10	1.518(16)	1.5498	C4	C5	C6	123.8(8)	120.286	C101	N14	Ag1	127.3(6)	129.249
C10	N3	1.55(3)	1.4826	N2	C6	C5	125.9(11)	122.563	C101	N14	C105	120.0	118.930
N13	C107	1.347(16)	1.4827	N2	C7	C8	89.8(11)	110.298	C105	N14	Ag1	112.6(6)	111.468
N13	C106	1.236(17)	1.2949	C7	C8	C9	123.5(12)	112.107	C102	C101	N14	120.0	121.893
N12	C111	1.291(16)	1.2949	C10	C9	C8	118.4(12)	112.108	C103	C102	C101	120.0	118.824
N12	Ag1A	2.312(15)	2.3333	C9	C10	N3	90.7(14)	110.299	C102	C103	C104	120.0	118.791
N12	C110	1.409(16)	1.4826	C107	N13	Ag1	125.1(13)	124.629	C103	C104	C105	120.0	119.078
N11	C112	1.3900	1.3658	C106	N13	Ag1	115.1(9)	115.580	N14	C105	C106	116.1(8)	117.821
N11	C116	1.3900	1.3518	C106	N13	C107	117.2(14)	119.791	C104	C105	N14	120.0	121.893
N11	Ag1A	2.411(13)	2.4542	C111	N12	Ag1A	114.3(9)	115.552	C104	C105	C106	123.8(8)	120.282
C112	C113	1.3900	1.4089	C111	N12	C110	119.2(12)	119.794	N13	C106	C105	123.4(11)	122.570
C112	C111	1.394(16)	1.4787	C110	N12	Ag1A	125.3(10)	124.653					
C113	C114	1.3900	1.4079	C112	N11	C116	120.0	118.932					
C114	C115	1.3900	1.4057	C112	N11	Ag1A	110.9(6)	111.485					
C115	C116	1.3900	1.4112	C116	N11	Ag1A	128.4(6)	129.228					
Ag1A	N4	2.414(12)	2.4535	N11	C112	C113	120.0	121.891					
Ag1A	N3	2.180(16)	2.3337	N11	C112	C111	117.8(9)	117.823					
N4	C12	1.3900	1.3658	C113	C112	C111	122.1(9)	120.282					
N4	C16	1.3900	1.3518	C114	C113	C112	120.0	119.079					
C12	C13	1.3900	1.4089	C115	C114	C113	120.0	118.824					
C12	C11	1.409(16)	1.4788	C114	C115	C116	120.0	118.791					
C13	C14	1.3900	1.4079	C115	C116	N11	120.0	122.482					
C14	C15	1.3900	1.4057	N12	C111	C112	124.0(12)	122.569					
C15	C16	1.3900	1.4112	N12	Ag1A	N11	72.0(5)	72.013					
C11	N3	1.230(18)	1.2949	N12	Ag1A	N4	109.8(5)	136.116					
C110	C109	1.488(16)	1.5498	N11	Ag1A	N4	147.2(6)	141.212					
C107	C108	1.530(16)	1.5499	N3	Ag1A	N12	163.7(7)	141.269					
C108	C109	1.494(14)	1.5445	N3	Ag1A	N11	114.7(5)	101.862					
N14	C101	1.3900	1.3518	N3	Ag1A	N4	73.1(5)	72.017					
N14	C105	1.3900	1.3658	C12	N4	Ag1A	108.0(6)	111.504					
C101	C102	1.3900	1.4112	C12	N4	C16	120.0	118.933					
C102	C103	1.3900	1.4057	C16	N4	Ag1A	131.6(6)	129.209					
C103	C104	1.3900	1.4079	N4	C12	C13	120.0	121.890					
C104	C105	1.3900	1.4089	N4	C12	C11	115.9(8)	117.822					
C105	C106	1.419(16)	1.4787	C13	C12	C11	124.1(8)	135.930					



Scheme 2. The synthesis of the complex I.

Molecular Hirshfeld surfaces are built based on electron distribution calculated as the sum of spherical atom electron densities [38,39]. Thus, an isosurface is obtained, and for each point of the isosurface, two distances can be defined:  $d_e$ , the distance from the point to the nearest atom outside to the surface, and  $d_i$ , the distance to the nearest atom inside to the surface. Furthermore, the identification of the regions of particular importance to intermolecular interactions is achieved by mapping normalized contact distance ( $d_{norm}$ ), expressed as:  $d_{norm} = (d_i - r_i^{vdw}) / r_i^{vdw} + (d_e - r_e^{vdw}) / r_e^{vdw}$ ; where  $r_i^{vdw}$  and  $r_e^{vdw}$  are the van der Waals radii of the atoms [40]. The value of  $d_{norm}$  is negative or positive when intermolecular contacts are shorter or longer than  $r^{vdw}$ , respectively. The graphical plots of the molecular Hirshfeld surfaces mapped with  $d_{norm}$  employ the red-white-blue color scheme, where red color indicates the shorter intermolecular contacts, the white color shows the contacts around the  $r^{vdw}$  separation, and blue color is used to point out the longer contact distances. Due to the symmetry between  $d_e$  and  $d_i$  in the expression for  $d_{norm}$ , where two Hirshfeld surfaces touch, both will display a red spot identical in color intensity as well as size and shape [41]. The mixture of  $d_e$  and  $d_i$  in the form of a 2D fingerprint plot provides a summary of intermolecular contacts in the crystal and are in complement to the Hirshfeld surfaces [40]. The information about the intermolecular interactions in the immediate environment of each molecule in the asymmetric unit is achieved by such plots. In addition, the close contacts between particular atom types can be highlighted in so-called resolved fingerprint plots [42], which allow the facile assignment of an intermolecular contact to a certain type of interaction and quantitatively summarize the nature and type of intermolecular contacts. Two additional colored properties (shape index and curvedness) based on the local curvature of the surface can also be specified [43]. The Hirshfeld surfaces are mapped with  $d_{norm}$ , shape-index, curvedness and 2D fingerprint plots (full and resolved) reported in this manuscript were generated using Crystal-Explorer 3.1 [44].

## 2.7. Molecular electrostatic potential (MEP)

The molecular electrostatic potential at a given point around a molecule can be defined in terms of total charge distribution of the molecule and related with the dipole moments. It supplies a method to understand the electron density which is useful for determining the electrophilic reactivity and nucleophilic reactivity along with hydrogen-bonding interactions [45,46].

## 3. Results and discussion

### 3.1. Synthetic aspects

The imino-pyridyl ligand **L** is a 1+2 condensates of 1,4-diaminobutane and 2-pyridine carboxaldehyde. The Ag(I) complex of **L** has been synthesized in good yields by reacting the AgClO<sub>4</sub> with the corresponding ligand at room temperature

in an equimolar proportion. The synthesis of the complex **I** has been summarized in Scheme 2. Complex **I** is stable in solid state for about 2-3 weeks in air and CH<sub>3</sub>OH and CH<sub>3</sub>CN solution for about 6 h.

### 3.2. IR and NMR spectroscopy

The complex **I** under study shows characteristic peaks due to the ligation of the ligand to the metal center in the KBr-phase IR spectra. In the IR spectrum of the ligand **L**, the characteristic band at 1649 cm<sup>-1</sup> is assigned to the imine (C=N) stretching frequencies. These bands due to C=N stretching have been shifted and appear at around 1615 cm<sup>-1</sup> in complex **I**. The bands due to ClO<sub>4</sub><sup>-</sup> ions appear at 1107 and 825 cm<sup>-1</sup> for complex **I**. The <sup>1</sup>H NMR spectra of the ligand **L** in CDCl<sub>3</sub> showed a singlet at  $\delta$  8.31 ppm due to (HC=N) proton, methylene protons resonates at  $\delta$  3.6 and 1.7 ppm. These protons appeared downfield for complex **I**.

### 3.3. Structural description of complex I

The X-ray crystallographic studies of complex **I** revealed that in the presence of Ag(I) ions, the ligand **L** gives rise to 20-membered macrocyclic dimer by Ag(I) grid (Figure 1). Two CH<sub>2</sub> groups in the asymmetric unit of complex **I** are disordered and located at three sites. For clarity, only one orientation of the four methylene groups are shown in Figure 1. In each complex, the tetradentate ligand binds the metal ion through two pyridine-N and two imine-N atoms. In the macrocyclic dimer **I**, each Ag(I) ion is tetra coordinated with two pyridine N-atoms and two imine N-atoms of the two different molecules of the spacer ligand **L**. Both the Ag(I) adopt distorted tetrahedral geometry. There exists weak Ag-Ag interaction having Ag-Ag separation of 5.318 Å along the chain. The Ag-N<sub>py</sub> distances fall in the range 2.335-2.426 Å and the Ag-N<sub>im</sub> distances fall in the range 2.180-2.312 Å (Table 2). The angles between the coordinating atoms centering Ag1 are 107.1(6), 72.6(4), 120.3(6), and 71.9(4)°, and Ag(I) sits 0.12 Å above the plane. The macrocyclic dimer in complex **I** supramolecularly arranged by  $\pi$ -stacking interactions. We have checked PLATON as well as Mercury, there are no Voids, if default probe radius of 1.2 Å is considered. In general, there are no classical H-bond in complex **I**.

### 3.4. Theoretical investigations

The optimized bond length and angles for the Ag(I) complex **I** are well replicated with the experimental single crystal X-ray diffraction structure data. Calculated bond parameters by DFT are consistent with the crystallographic data of complex **I** and are given in Table 2. The calculated metal ligand bonds Ag1-N1, Ag1-N2, Ag1-N13, and Ag1-N14 bond distances are a little bit longer than their respective X-ray crystallographic data. For complex **I**, the computed angles have less than  $\pm 3^\circ$  deviation from their respective experimental values.

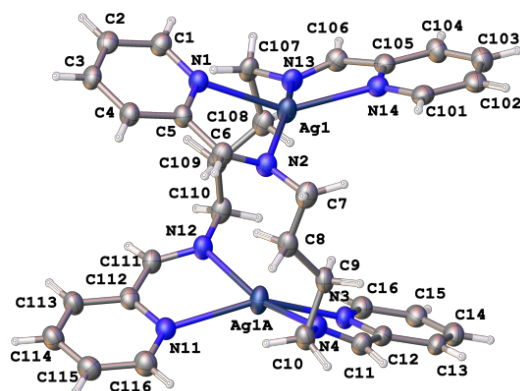


Figure 1. Molecular structure of  $[Ag_2(\mu L)_2](ClO_4)_2$  (I).

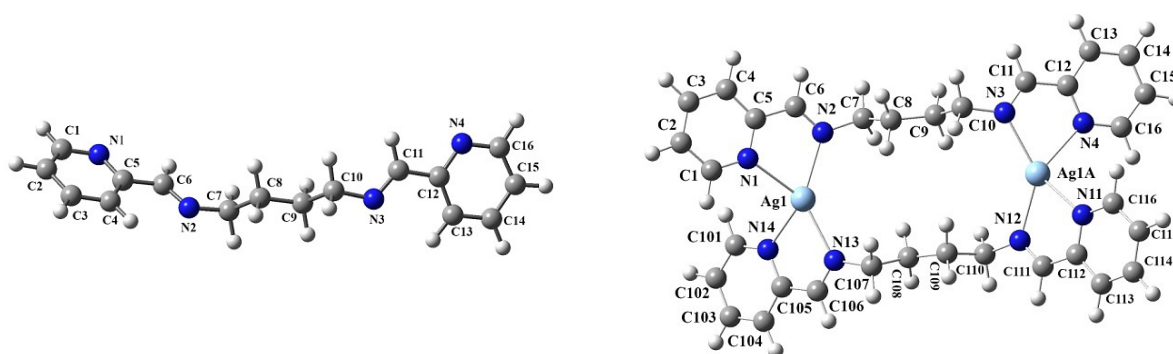


Figure 2. Optimized molecular structure of the ligand L and complex I.

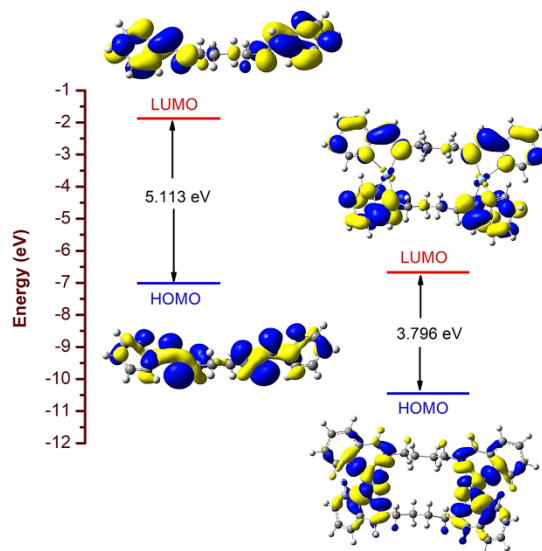


Figure 3. Surface plots of HOMO and LUMO of the ligand L and Ag(I) complex I.

The optimized bond parameters of free ligand (L) and both optimized as well as experimental bond parameters of coordinated ligand are almost same. Thus, our calculated bond lengths and angles are in agreement with the experimental data. The overall variations are reasonable, since the performed quantum mechanical optimization is not exactly comparable with the experimental data as it was carried out in vacuum at 0 K. Thus, the deviation of the calculated bond parameters from the experimental data may arise due to conformational changes induced by the crystal field and temperature effect as well as the basis sets chosen for calculations [47]. The optimized

structure of ligand L and the Ag(I) complex I have been shown in Figure 2. The surface plots of HOMO and LUMO of the ligand L and complex I have been depicted in Figure 3.

### 3.5. Molecular Hirshfeld surfaces

The Hirshfeld surface is a suitable tool for describing the surface characteristics of molecules. The molecular Hirshfeld surface of complex I was generated using a standard (high) surface resolution with the 3D  $d_{norm}$  surfaces mapped over a fixed color scale of -0.22 (red) to 1.4 Å (blue).



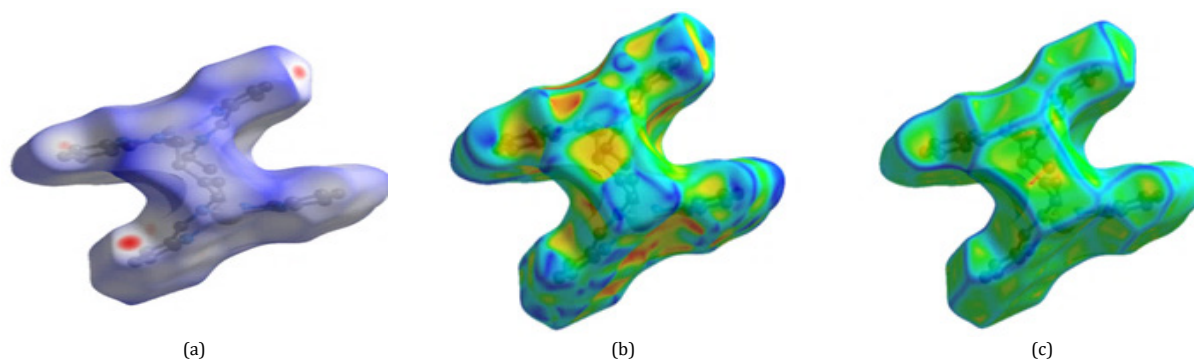


Figure 4. Hirshfeld surfaces of complex I, (a) 3D  $d_{norm}$  surface, (b) shape index, (c) curvedness.

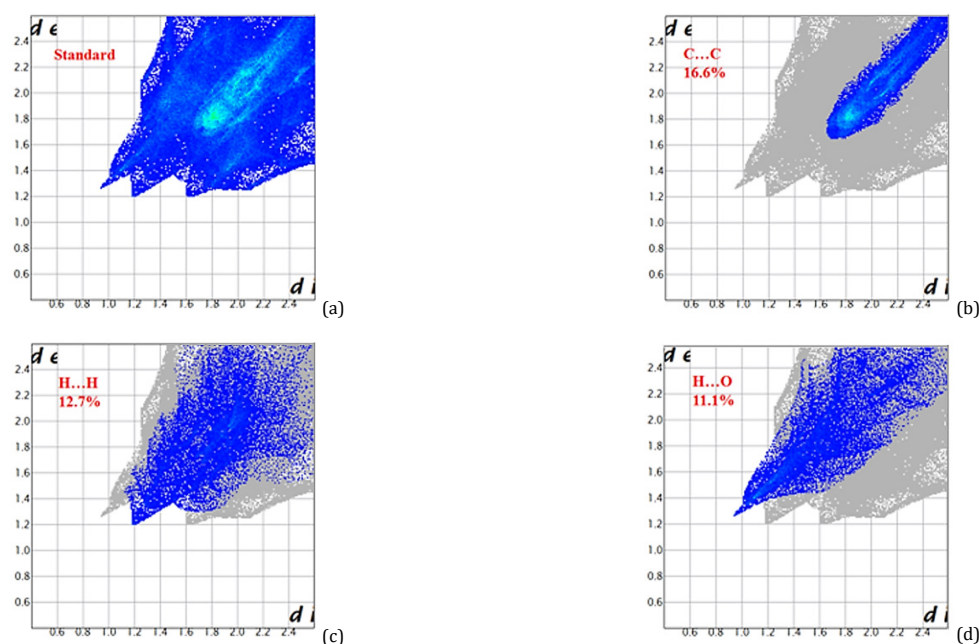


Figure 5. 2D fingerprint plots of complex I: (a) standard full and (b) resolved into C...C and (c) resolved into H...H (d) O...H contacts, showing the percentages of contacts contributing to the total Hirshfeld surface area of the molecule.

The shape index mapped in the color range of -0.99 to 1.0, and Curvedness was in the range of -4.0 to 0.4. The surfaces were shown to be transparent to allow visualization of the molecular moiety in a similar orientation for all of the structures around which they were calculated. The molecular Hirshfeld surface ( $d_{norm}$ , Shape index and Curvedness) of complex I has been shown in Figure 4.

The Hirshfeld surface analysis of complex I shows that C...C, H...H, and O...H interactions of 16.6, 12.7, and 11.1%, respectively, which revealed that the main intermolecular interactions were C...C intermolecular interactions. Both the H...H and O...H interactions were represented almost same area by a small area in the right side of the top in the 2D fingerprint map, whereas the C...C interactions were represented by the largest in the fingerprint plot (Figure 5) and thus had the most significant contribution to the total Hirshfeld surfaces (16.6 %).

### 3.6. Molecular electrostatic potential (MEP)

The potential increases in the order red < yellow < green < blue < pink < white. Red and yellow represent the regions of most negative electrostatic potential which is related to electrophilic reactivity, white represents the region of most positive electrostatic potential which is related to nucleophilic reactivity and blue represents the region of zero potential.

Molecular electrostatic potential (MEP) of ligand L has been shown in Figure 6.

### 3.7. Photophysical studies

Photoluminescence properties of  $d^{10}$  metal coordination compounds have been extensively studied due to their potential applications as luminescent materials. Coordination compounds have been reported to have ability to adjust the emission wavelength of organic substances through the incorporation of metal centers and the anions. Therefore, it is important to investigate the luminescence properties of coordination compounds in view of their potential applications as light-emitting diodes (LEDs). The luminescent behaviors of the ligand and its complex I have been studied in the  $\text{CH}_3\text{CN}$  solution at room temperature with the emission maxima at 448 nm. Intense photoluminescence was observed only for complex I and the ligand L does not show any emission (Figure 7).

The mechanism of fluorescence properties of complex I can be predicted by TD-DFT calculations. The energy gap between the highest occupied molecular orbital (HOMO) and the lowest unoccupied molecular orbital (LUMO) of L and I is 5.113 and 3.796 eV, respectively. The silver complex I compared to L are established to exhibit an easy electronic transition, resulting in their further stability (Figure 3).

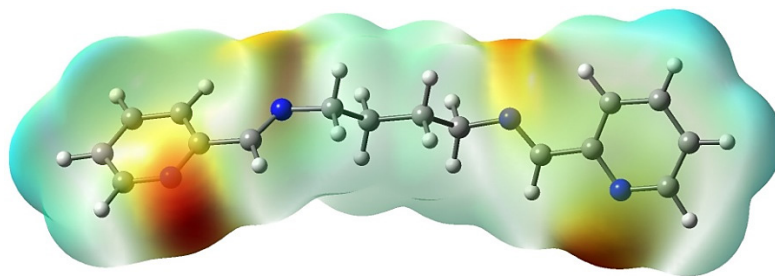


Figure 6. Molecular electrostatic potential of **L**.

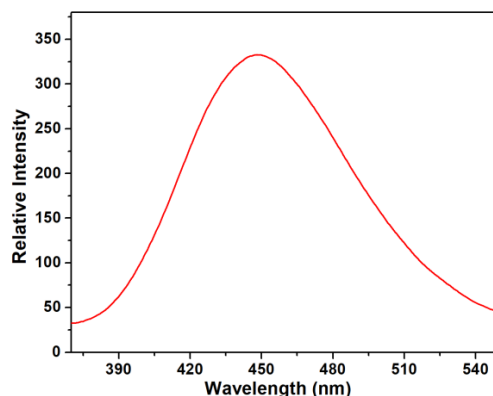


Figure 7. Emission spectra of complex **I** in acetonitrile at room temperature with excitation at 340 nm.

The contours of the electronic distribution in the HOMO and LUMO states of these molecules suggest significant energy difference of 1.317 eV between **L** and **I**. The **L** is not response to photoluminescent but its Ag(I) complex displays photoluminescence excited at 340 nm. The contours of HOMO and LUMO of complex **I** clearly show chelation of **L** with Ag(I). The origin of the fluorescence properties of **I** probably because of the CHEF (chelation-enhanced fluorescence) processes [48].

#### 4. Conclusion

Herein, a *bis* Schiff base imino pyridyl ligand **L** and its dimeric silver(I) complex **I** have been reported. Complex **I** represents a 20-membered macrocyclic cage via Ag(I) grid with the imino-pyridyl ligand **L**. A somewhat distorted tetrahedral geometry around each Ag(I) has been observed in its X-ray single crystal structure. DFT studies reveals that the energy gap between the highest occupied molecular orbital (HOMO) and the lowest unoccupied molecular orbital (LUMO) of **L** and [Ag<sub>2</sub>L<sub>2</sub>]<sup>2+</sup> (**I**) is 5.113 and 3.796 eV, respectively. The contours of the electronic distribution in the HOMO and LUMO states of these molecules suggest a significant energy difference of 1.317 eV between **L** and **I**. The ligand **L** is non-photoluminescent, but its Ag(I) complex (**I**) displays photoluminescence on excitation at 340 nm with the emission maxima at 450 nm; which is supposed to be because of the easy electronic transition. The Hirshfeld surface analysis of complex **I** show that C...C, H...H, and O...H interactions of 16.6, 12.7, and 11.1%; respectively, which exposed that the main intermolecular interactions were C...C intermolecular interactions. There is no void, if default probe radius of 1.2 Å is considered. In general, there is no classical H-bond in the complex **I**.

#### Acknowledgements

Goutam Kumar Patra would like to thank the Department of Science and Technology (SR/FST/CSI-264/2014 and EMR/2017/0001789) and Department of Biotechnology, Govern-

ment of India, New Delhi for financial support. Meman Sahu thanks the Council for Scientific and Industrial Research, Government of India, for financial support in the form of research fellowships.

#### Supporting information

CCDC-2058296 contains the supplementary crystallographic data for this paper. These data can be obtained free of charge via <https://www.ccdc.cam.ac.uk/structures/>, or by e-mailing [data\\_request@ccdc.cam.ac.uk](mailto:data_request@ccdc.cam.ac.uk), or by contacting The Cambridge Crystallographic Data Centre, 12 Union Road, Cambridge CB2 1EZ, UK; fax: +44(0)1223-336033.

#### Disclosure statement

Conflict of interests: The authors declare that they have no conflict of interest.

Author contributions: All authors contributed equally to this work.

Ethical approval: All ethical guidelines have been adhered.

Sample availability: Samples of the compounds are available from the author.

#### ORCID

Jahangir Mondal

 <https://orcid.org/0000-0001-9867-5193>


Memansahu

 <https://orcid.org/0000-0001-9397-4805>

Bhaskar Sharma

 <https://orcid.org/0000-0001-7944-4955>

Rakesh Ganguly

 <https://orcid.org/0000-0002-9523-6918>

Shubhamoy Chowdhury

 <https://orcid.org/0000-0003-1545-9693>

Goutam Kumar Patra

 <https://orcid.org/0000-0003-3151-0284>

## References

- [1]. Yamada, S. *Coord. Chem. Rev.* **1999**, 190–192, 537–555.
- [2]. Wang, X.; Qin, C.; Wang, E.; Li, Y.; Hao, N.; Hu, C.; Xu, L. *Inorg. Chem.* **2004**, 43 (6), 1850–1856.
- [3]. Qin, C.; Wang, X.; Wang, E.; Xu, L. *J. Mol. Struct.* **2005**, 738 (1–3), 91–98.
- [4]. Wen, L.; Li, Y.; Dang, D.; Tian, Z.; Ni, Z.; Meng, Q. *J. Solid State Chem.* **2005**, 178 (11), 3336–3341.
- [5]. Majumder, A.; Rosair, G. M.; Mallick, A.; Chattopadhyay, N.; Mitra, S. *Polyhedron* **2006**, 25 (8), 1753–1762.
- [6]. Muthu, S.; Ni, Z.; Vittal, J. J. *Inorg. Chim. Acta* **2005**, 358 (3), 595–605.
- [7]. Yue, S.-M.; Xu, H.-B.; Ma, J.-F.; Su, Z.-M.; Kan, Y.-H.; Zhang, H.-J. *Polyhedron* **2006**, 25 (3), 635–644.
- [8]. Carlucci, L.; Ciani, G.; Proserpio, D. M. *Coord. Chem. Rev.* **2003**, 246 (1–2), 247–289.
- [9]. Beauvais, L. G.; Long, J. R. *Inorg. Chem.* **2006**, 45 (1), 236–243.
- [10]. Chandler, B. D.; Cramb, D. T.; Shimizu, G. K. H. *J. Am. Chem. Soc.* **2006**, 128 (32), 10403–10412.
- [11]. Gu, Z.-G.; Fang, H.-C.; Yin, P.-Y.; Tong, L.; Ying, Y.; Hu, S.-J.; Li, W.-S.; Cai, Y.-P. *Cryst. Growth Des.* **2011**, 11 (6), 2220–2227.
- [12]. Dybtsev, D. N.; Chun, H.; Yoon, S. H.; Kim, D.; Kim, K. J. *Am. Chem. Soc.* **2004**, 126 (1), 32–33.
- [13]. Rao, C. N. R.; Natarajan, S.; Vaidyanathan, R. *Angew. Chem. Int. Ed Engl.* **2004**, 43 (12), 1466–1496.
- [14]. Lee, J.-Y.; Chen, C.-Y.; Lee, H. M.; Passaglia, E.; Vizza, F.; Oberhauser, W. *Cryst. Growth Des.* **2011**, 11 (4), 1230–1237.
- [15]. Eddaoudi, M.; Moler, D. B.; Li, H.; Chen, B.; Reineke, T. M.; O’Keeffe, M.; Yaghi, O. M. *Acc. Chem. Res.* **2001**, 34 (4), 319–330.
- [16]. Moulton, B.; Zaworotko, M. J. *Chem. Rev.* **2001**, 101 (6), 1629–1658.
- [17]. Janiak, C. *Dalton Trans.* **2003**, 14, 2781–2804.
- [18]. Roesky, H. W.; Andruh, M. *Coord. Chem. Rev.* **2003**, 236 (1–2), 91–119.
- [19]. Luan, X.-J.; Wang, Y.-Y.; Li, D.-S.; Liu, P.; Hu, H.-M.; Shi, Q.-Z.; Peng, S.-M. *Angew. Chem. Int. Ed Engl.* **2005**, 44 (25), 3864–3867.
- [20]. Ding, B.-B.; Weng, Y.-Q.; Mao, Z.-W.; Lam, C.-K.; Chen, X.-M.; Ye, B.-H. *Inorg. Chem.* **2005**, 44 (24), 8836–8845.
- [21]. Angeloni, A.; Crawford, P. C.; Orpen, A. G.; Podesta, T. J.; Shore, B. J. *Chemistry* **2004**, 10 (15), 3783–3791.
- [22]. Balamurugan, V.; Hundal, M. S.; Mukherjee, R. *Chemistry* **2004**, 10 (7), 1683–1690.
- [23]. Braga, D.; Grepioni, F.; Desiraju, G. R. *Chem. Rev.* **1998**, 98 (4), 1375–1406.
- [24]. Janiak, C.; Scharmann, T. G. *Polyhedron* **2003**, 22 (8), 1123–1133.
- [25]. Pal, S.; Pal, S. *Polyhedron* **2003**, 22 (6), 867–873.
- [26]. Patra, G. K.; Pal, P. K.; Mondal, J.; Ghorai, A.; Mukherjee, A.; Saha, R.; Fun, H.-K. *Inorg. Chim. Acta* **2016**, 447, 77–86.
- [27]. Mondal, J.; Mukherjee, A.; Patra, G. K. *Inorg. Chim. Acta* **2017**, 463, 44–53.
- [28]. Mondal, J.; Pal, P. K.; Mukherjee, A.; Patra, G. K. *Inorg. Chim. Acta* **2017**, 466, 274–284.
- [29]. Bruker (2008). SAINT, SMART. Bruker AXS Inc., Madison, Wisconsin, USA.
- [30]. Sheldrick, G. M. *Acta Crystallogr. A* **2008**, 64 (1), 112–122.
- [31]. Farrugia, L. J. *J. Appl. Crystallogr.* **1999**, 32 (4), 837–838.
- [32]. Frisch, M. J.; Trucks, G. W.; Schlegel, H. B.; Scuseria, G. E.; Robb, M. A.; Cheeseman, J. R.; Scalmani, G.; Barone, V.; Mennucci, B.; Petersson, G. A.; Nakatsuji, H.; Caricato, M.; Li, X.; Hratchian, H. P.; Izmaylov, A. F.; Bloino, J.; Zheng, G.; Sonnenberg, J. L.; Hada, M.; Ehara, M.; Toyota, K.; Fukuda, R.; Hasegawa, J.; Ishida, M.; Nakajima, T.; Honda, Y.; Kitao, O.; Nakai, H.; Vreven, T.; Montgomery, J. A.; Peralta, J. E.; Ogliaro, F.; Bearpark, M.; Heyd, J. J.; Brothers, E.; Kudin, K. N.; Staroverov, V. N.; Kobayashi, R.; Normand, J.; Raghavachari, K.; Rendell, A.; Burant, J. C.; Iyengar, S. S.; Tomasi, J.; Cossi, M.; Rega, N.; Millam, J. M.; Klene, M.; Knox, J. E.; Cross, J. B.; Bakken, V.; Adamo, C.; Jaramillo, J.; Gomperts, R.; Stratmann, R. E.; Yazyev, O.; A. J. Austin, A. J.; Cammi, R.; Pomelli, C.; Ochterski, J. W.; Martin, R. L.; Morokuma, K.; Zakrzewski, V. G.; Voth, G. A.; Salvador, P.; Dannenberg, J. J.; Dapprich, S.; Daniels, A. D.; Farkas, O.; Foresman, J. B.; Ortiz, J. V.; Cioslowski, J.; Fox, D. J. Gaussian, Inc., Gaussian 09, Revision A. 02, Wallingford CT, 2009.
- [33]. Dennington, R.; Keith, T.; Millam, J.; Gaussview. *Version 5*; Semichem Inc: Shawnee Mission, KS, 2009.
- [34]. Hay, P. J.; Wadt, W. R. *J. Chem. Phys.* **1985**, 82 (1), 299–310.
- [35]. Barone, V.; Cossi, M. *J. Phys. Chem. A* **1998**, 102 (11), 1995–2001.
- [36]. Tomasi, J.; Mennucci, B.; Cammi, R. *Chem. Rev.* **2005**, 105 (8), 2999–3093.
- [37]. Norret, M.; Makha, M.; Sobolev, A. N.; Raston, C. L. *New J. Chem.* **2008**, 32 (5), 808–812.
- [38]. Spackman, M. A.; McKinnon, J. J. *CrystEngComm* **2002**, 4 (66), 378–392.
- [39]. Meng, X. X. Applications of Hirshfeld surfaces to ionic and mineral crystals, Ph.D. Thesis, University of New England, 2004.
- [40]. Pendás, A. M.; Luaña, V.; Pueyo, L.; Francisco, E.; Mori-Sánchez, P. *J. Chem. Phys.* **2002**, 117 (3), 1017–1023.
- [41]. Hyde, S.; Andersson, S.; Larsson, K.; Blum, Z.; Landh, T.; Lidin, S.; Ninham, B. W. *The Language of Shape*; Elsevier: Amsterdam, 1997.
- [42]. Nishikawa, M.; Nomoto, K.; Kume, S.; Inoue, K.; Sakai, M.; Fujii, M.; Nishihara, H. *J. Am. Chem. Soc.* **2010**, 132 (28), 9579–9581.
- [43]. Desiraju, G. R. *Angew. Chem. Int. Ed Engl.* **2007**, 46 (44), 8342–8356.
- [44]. Schmidt, G. M. J. *Pure Appl. Chem.* **1971**, 27 (4), 647–678.
- [45]. Sebastian, S.; Sundaraganesan, N. *Spectrochim. Acta A Mol. Biomol. Spectrosc.* **2010**, 75 (3), 941–952.
- [46]. Luque, F. J.; López, J. M.; Orozco, M. *Theor. Chem. Acc.* **2000**, 103 (3–4), 343–345.
- [47]. Bhattacharya, A.; Naskar, J. P.; Majumder, S.; Ganguly, R.; Mitra, P.; Chowdhury, S. *Inorg. Chim. Acta* **2015**, 425, 124–133.
- [48]. Sahu, M.; Manna, A. K.; Chowdhury, S.; Patra, G. K. *RSC Adv.* **2020**, 10 (73), 44860–44875.



Copyright © 2021 by Authors. This work is published and licensed by Atlanta Publishing House LLC, Atlanta, GA, USA. The full terms of this license are available at <http://www.eurjchem.com/index.php/eurjchem/pages/view/terms> and incorporate the Creative Commons Attribution-Non Commercial (CC BY NC) (International, v4.0) license (<http://creativecommons.org/licenses/by-nc/4.0>). By accessing the work, you hereby accept the Terms. This is an open access article distributed under the terms and conditions of the CC BY NC License, which permits unrestricted non-commercial use, distribution, and reproduction in any medium, provided the original work is properly cited without any further permission from Atlanta Publishing House LLC (European Journal of Chemistry). No use, distribution or reproduction is permitted which does not comply with these terms. Permissions for commercial use of this work beyond the scope of the License (<http://www.eurjchem.com/index.php/eurjchem/pages/view/terms>) are administered by Atlanta Publishing House LLC (European Journal of Chemistry).